

Glaucoma Detection with Improved Deep Learning Model Trained with Optimal Features: An Improved Meta-Heuristic Model

^{1*}Raja Chandrasekaran, ² Santhosh Krishna B V, ³Balaji Loganathan,
⁴Sanjay Kumar Suman, ⁵Bhagyalakshmi

Submitted: 11/02/2023 **Revised:** 12/04/2023 **Accepted:** 10/05/2023

Abstract—Glaucoma is by far the most common retinal condition, wherein the intraocular pressure (IOP) on the eye damages the retina. Glaucoma damages ONH, which leads to visual impairment if not addressed. A skilled ophthalmologist checks the course of glaucoma on the retinal area of the eye. This method is time-consuming and inefficient. As a result, this is indeed a legitimate problem that can be addressed by using deep learning algorithms to automatically diagnose glaucoma. In this research work, a novel glaucoma detection model is developed by following five major phases: “(a) pre-processing, (b) ROI identification, (c) feature extraction, (d) feature selection, and (e) glaucoma classification (normal / diseased)”. Initially, the collected retinal images are pre-processed via Wiener filtering (to remove noise) and CLAHE (for contrast enhancement). Then, ROI of pre-processed image is selected via Optimized K-Means clustering technique, wherein the centroids of K-means are optimally selected via Dingo with Enhanced Encircling Optimization Model (DEEO). Subsequently, the features inclusive of color feature (Color Histogram and Color Co-occurrence Matrix (CCM)), texture features (Local Binary Pattern-LBP, Median Local Gradient Pattern-MLGP) are extracted from the identified ROI areas. Further, among the selected features, the most relevant features are selected via Dingo with Enhanced Encircling Optimization Model (DEEO). This DEEO is a conceptual expansion of standard Dingo Optimizer (DOX). Ultimately, using Improved CNN (I-CNN), the classification of OC and OD for healthy and diseased takes place precisely. Finally, a comparative evaluation is undergone to validate the efficiency of the projected model.

Keywords—Glaucoma; Fundus Eye; OD and OC; Optimized K-Means clustering technique; Median Local Gradient Pattern-MLGP; DEEO; I-CNN

Nomenclature

Abbreviation	Description
MRI	Magnetic Resonance Imaging
ONH	Optic Nerve Head
LBP	Local Binary Pattern
DEEO	Dingo with Enhanced Encircling Optimization Model
OC	optic cup
LGP	Local Gradient Pattern
ROI	Region of Interest
CLAHE	Contrast Limited Adaptive Histogram Equalization
DOX	Dingo Optimizer
CCM	Color Co-occurrence Matrix
I-CNN	Improved CNN model
CDR	Cup-to-Disc-Ratio

¹Associate Professor, Department of ECE, Vel Tech Rangarajan Dr. Sagunthala R & D Institute of Science and Technology, Chennai, Tamil Nadu, India

² Associate Professor, Department of CSE, New Horizon College of Engineering, Bengaluru, Karnataka, India

³Associate Professor, Department of ECE, Vel Tech Rangarajan Dr. Sagunthala R & D Institute of Science and Technology, Chennai, Tamil Nadu, India

⁴Professor, Department of ECE, St. Martin's Engineering College, Telangana, India

⁵Professor, Department of ECE, Rajalakshmi Engineering College, Chennai, Tamil Nadu, India

*Corresponding author mail: rajachandru82@gmail.com

IOU	Intersection over Union
AHE	Adaptive Histogram Equalization
OD	Optical Disc
MLGP	Median Local Gradient Pattern
OCT	Optical Coherence Tomography
MBE	Mean Bias Error

Introduction

“Glaucoma” is often termed as the "silent thief of sight" as it's the primary factor of loss of vision worldwide [1] [2] [3][4] [5]. Glaucoma affects more than “60 million people worldwide”, with the figure estimated to rise to 79.6 million by 2020. Glaucoma can cause changes with in retinal structure. Glaucoma is caused mostly by ONH structural alterations within that retina [6][7][8][9]. Glaucoma produces a serious issue with the optic nerve, which results in a constant deterioration of eyesight if it is not treated properly [10] [11] [12]. Early detection of glaucoma in its initial phases has therefore significantly reduced the risk of irreversible vision loss [13][14][15]. With the aid of the retinal nerve fibres located just on OD, the images collected from the retina will indeed be transformed to visual cues and delivered towards the brain. Photoreceptors such as cones and rods can be found in the OD of the retina, which aid eyesight. OD dubbed it the "blind spot" just because of that [16] [17][18][19]. The OC, which seems to be the brightest portion of the retina, is found at the very end of the OD. In healthy people, an OC covers around 30percent of the overall of the disc.

Fundus imaging, MRI, OCT, and other image modalities will be utilised to identify glaucoma [20][21][22] [23] [24][25]. However, fundus images are taken into account for glaucoma identification

throughout the suggested method. The fundus images are images of the retina that are taken using a fundus camera. The "macula, optic disc, fovea, optic cup, artery, veins, and other components" of the retina may be seen clearly in fundus pictures [25][26][27][28]. It's been shown that fundus scans can be used to detect eye disorders fast. The OD, which contains an “OC and neuroretinal rim”, is perhaps the brightest area of the retina in fundus imaging. The OC seems to be the inner section of the OD, while the OC's outer limit is the “neuroretinal rim”. Optic cupping arises as the diameter of the OC grows larger [29] [30][31]. Glaucoma can indeed be recognised by locating the optic nerve cupping. Numerous metrics would be utilised to diagnose glaucoma, however the “cup-to-disc-ratio” number is just the best diagnostic. The CDR seems to be the gap between OD and the OC. Glaucoma is diagnosed when the diameter of the OC rises more than just the real size [31][32][33] [34][35] [36].

The segmentation of OD and OC is required to get the CDR ratio, however current manual procedures take much longer and produce inconsistent data. As a result, glaucoma diagnosis relies heavily on automated segmentation of the OC and OC. OD and OC are represented by dotted lines in Fig. 1 to indicate a normal healthy eye and a “glaucoma suspicious eye” [37][38][39].

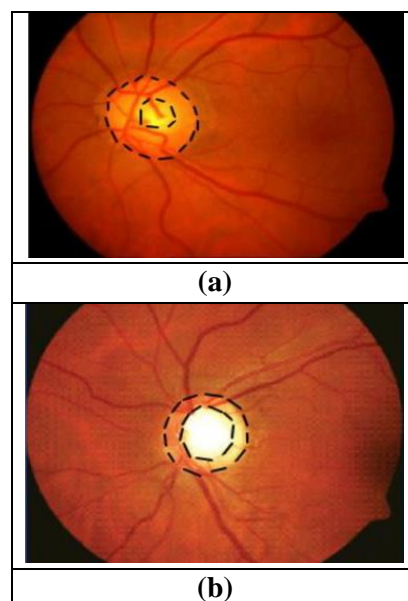


Fig. 1. Sample image : (a) Healthy eye and (b) Glaucomatous eye

As a result, early illness identification can help people avoid becoming blind [3]. So, grouping the harmful region seems beneficial for not only the ophthalmologist's further thorough medical assessment, as well as for the building of computerized illness classification systems [4]. Researchers first detect problems in the eyes by manually inspecting glaucoma locations and estimating CDR, size, and border deviations [5]. However, owing to a scarcity of professionals, prompt discovery of the eye anomaly is often prolonged [6], despite the fact that early diagnosis and treatment of the condition might save the perpetrator's sight. To address the aforementioned issues, scientists are focusing on illness detection using CAD-based technologies. "Image pre-processing, feature extraction, feature selection, segmentation", and eventually classification are all part of the automated detection approach [40] [41] [42] [43] [44] [45]. The first phase is pre-processing, which involves removing noise and anomalies from the photograph in order to enhance clarity. many morphological procedures are employed for "feature extraction and feature selection", followed by diverse algorithms for classification. Numerous approaches for detecting glaucoma depending on multiple retinal image modalities have been developed based on current methodology [46] [47]. The deep learning technology would be used to diagnose glaucoma inside the suggested method.

The key contribution of this research work is manifested below:

1. To identify the ROI region in the fundus image using the newly projected Optimized K-Means clustering technique, wherein the centroids of K-means are optimally selected via Dingo with Enhanced Encircling Optimization Model (DEEO).
2. To select the Median Local Gradient Pattern-MLGP based features along with other colour as well as texture features for training the model.
3. To select the optimal features with Dingo with Enhanced Encircling Optimization Model (DEEO).
4. To classify OC and OD for healthy and diseased glaucoma patients using the newly projected Improved Convolutional Neural Network model (I-CNN), wherein MBE loss function is used for efficient image classification
5. To introduce a new DEEO model for efficient centroid selection as well as optimal feature selection. This DEEO model is an improved version of standard DOX.

The remainder of this research is organised as follows: The second section highlights current and exciting work on detecting glaucoma using retinal fundus pictures. The suggested Glaucoma Detection Model with Improved Deep Learning Model is discussed in Section III. In Section IV, the results obtained with the projected model are thoroughly explored. Section V brings the paper to a conclusion.

Literature Review

Related works

In 2021, *et al.* [1] have developed a simple glaucoma master framework for segmenting the optic cup and disc and calculating CDR. Deep learning and innovative CNN have been used to diagnose glaucoma in this case. To get a more accurate outcome, the suggested method segments the OC and OD using two distinct CNN architectures. This classifier was tested as well as evaluated using the publically available "DRISHTI – GS database", and it obtained a "segmentation accuracy of 98 percent for the optic disc and 97 percent for the optic cup". However, the sensitivity as well as specificity of the model is lower. Moreover, the computational complexity of the model needs to be increased in terms of training time.

In 2021, Tulsani *et al.* [2] have devised an unique method for detecting glaucoma by segmenting the optic disc and cup. To boost performance on a limited dataset, the Dhristi dataset has been employed. Again for segmentation task, a bespoke UNET++ model with hyper-parameter tuning and a custom loss tool has been developed. Due to the very small size of the optic nerve head, the established loss function aids in combating the class imbalance. Based on clinical feature detection, the suggested method obtained 96% accuracy in categorising "glaucomatous and non-glaucomatous images". The improved model achieves IOU values of 0.9477 for the optic disc and 0.9321 for the optic cup, as well as a reduction in training time. This research work is applicable only for small image set, and hence it is not applicable for real-time processing. Moreover, this model is prone to errors.

In 2021, Liu *et al.* [3] suggested a new unsupervised approach that relies on "adversarial learning" that accomplish the OD and OC "segmentation and glaucoma diagnostic functions" quite generalised as well as effectively. To handle the issue of domain shift, researchers have used an efficiency segmentation and classification model and "unsupervised domain adaptation technology" on the output sequence of the segmentation model. To

generate more consistent and effective glaucoma screening prediction, they incorporated classification and segmentation networks. Using three public datasets, the "REFUGE, DRISHTI-GS, and RIM-ONE-r3 datasets", they demonstrate the usefulness and efficiency of our suggested techniques. On the other hand, the complexity of the model is higher in terms of memory consumption as well as time consumption. In addition, this model recorded less sensitivity (82%), which is indeed a major drawback of this research.

In 2020, Mvoulana *et al.* [4] proposed a novel entirely automated glaucoma screening and diagnostic system based on retinal fundus images. They have been concentrating their research just on construction of such a cognitively accurate method for intended to create and maintain on portable equipment in order to provide ocular inspection in distant places having restricted access to medical services. Firstly, the framework incorporates a "brightness criterion and a template matching" methodology to successfully distinguish the OD even in the presence of bright lesions consistent with diseased instances. Then, utilising a "texture-based and model-based technique", an efficient OC and OD segmentation has been achieved. Finally, CDR has been used to do glaucoma screening and classify individuals as healthy or glaucomatous. The classification rate has been identified to be lower, and it's not sufficient for large database.

In 2021, Escorcia-Gutierrez *et al.* [5] developed a unique colour hybrid approach using an OD detection technique cantered on Markowitz's Modern Portfolio Theory. The training phase, determines the best weights for every colour channel. In the testing phase, a fusion of weighted colour channels has been used. To estimate the performance of the model, two distinct segmentation approaches have been provided and evaluated with extant computer vision techniques. A lower level of accuracy and overlap (0.8 and 80%, respectively) has been recorded, and this is the major drawback of this approach.

As per the literature review undergone, the classification accuracy of OC and OD has been identified as a major challenge that needs to be overridden. Moreover, the sensitivity as well as specificity of the existing models has also identified to be lower. This research work intends to fill this gap by developing a novel improved deep learning approach.

Proposed Galucoma Detection Model with Improved Deep Learning Model

Architectural Description

Glaucoma is indeed a serious ocular ailment that damages OD and OC, eventually leads to loss of vision. The disease displays a mild range of symptoms mostly in early phases due to its own sluggish progression, making diagnosis and treatment difficult. As a result, a completely automated approach is required to assist in the screening process and raise the probability of earlier disease diagnosis. A new glaucoma detection model is developed. The proposed glaucoma detection approach contains five primary phases: "(a) pre-processing, (b) ROI identification, (c) feature extraction, (d) feature selection, and (e) glaucoma classification (normal / diseased)". The architecture of the projected model is shown in Fig.2. The acquired raw pictures (retinal portion of the eye) will be indicated as img^{inp} , and is further processed to detect glaucoma early.

The following are the steps undertaken in the proposed early glaucoma detection model:

Step1: img^{inp} is first pre-processed using wiener filtering (to remove noise) and CLAHE (for contrast enhancement). The noise in img^{inp} is eliminated, and the contrast of the noise-free images is subsequently improved. The result obtained after the contrast removal is denoted by the symbol img^{pre} (pre-processed image).

Step2: Next, using an Optimized K-Means clustering technique, the ROI region in img^{pre} is identified(proposed). The new Dingo with Enhanced Encircling Optimization Model (DEEO), which is a conceptual upgrade of the regular Dingo Optimization (DOX) Model, is used to determine the centroid of the K-means of the model. As a resultant, the ROI region is isolated from img^{pre} . img^{ROI} denotes the ROI region that has been segregated from the non-ROI region img^{ROI-N} .

Step3: The features inclusive of colour feature $g(color)$, texture features $g(texture)$ (LBP (LBP) and Median Local Gradient Pattern (MLGP)) are extracted from img^{ROI} . These extracted features are together denoted as $G = g(texture) + g(color)$

Step4: Among G there is certain irrelevant features, and these might diminish the

performance of the model based on computational complexity (time and memory). Therefore, the optimal features among G are selected via Dingo with Enhanced Encircling Optimization Model (DEEO). These optimally selected features are pointed as G^{opt} .

Step5: The classification of OC and OD for healthy and diseased takes place at this stage. The classification is accomplished via Improved CNN model (I-CNN). This Improved CNN is trained with G^{opt} . As a resultant, the outcome from Improved CNN exhibits the state of OC and OD (i.e. diseased or healthy).

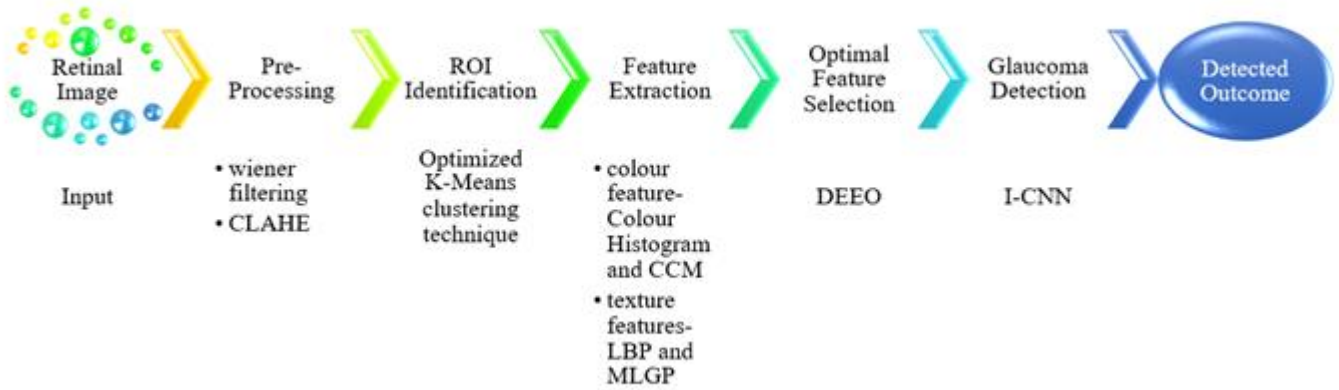


Fig. 2. Block Diagram of the projected Glaucoma detection model with improved deep learning model

Pre-Processing

The pre-processing is indeed the most basic step for image processing. In this research work, the collected raw images corresponding to OC img^{inp} are pre-processed via Wiener filtering [49] and CLAHE [50]. This phase is diagrammatically shown in Fig.3. Initially, the noises within img^{inp} are removed via wiener filtering, and this noise removed images is pointed as $img^{noisefree}$. This $img^{noisefree}$ images are enhanced in terms of contrast via CLAHE model. The outcome from CLAHE is a pre-processed image img^{pre} .

Weiner Filtering: The collected input image (retinal part of the eye) img^{inp} is subjected to Wiener filtering model. The Wiener filter is perhaps the most significant method for removing blur in images caused by linear movement or unfocused optics. Blurring in an image caused by linear motion is indeed the result of poor sampling from an image processing perspective. A single fixed point at the front of the camera should be represented from each pixel in a digital form of the picture.

Mathematically, the Weiner filtering applied onto img^{inp} having pixels (a, b) can be represented as per Eq. (1).

$$img^{noisefree} = G(a, b) = F(a, b).H(a, b) \quad (1)$$

Here, $G(a, b)$ is the noiseless image acquired after filtering and $F(a, b)$ is the filtered image and

$H(a, b)$ is the blurring function. The noise removed image is pointed as $img^{noisefree}$.

CLAHE: The contrast of $img^{noisefree}$ is enhanced via CLAHE, which is a variation of AHE that compensates for contrast over amplification. CLAHE works on tiles, which are tiny areas of the image rather than the complete image. After that, bilinear blending is used to mix the tiles that are next to each other. The contrast enhanced image is represented as img^{pre} , which is the pre-processed image.

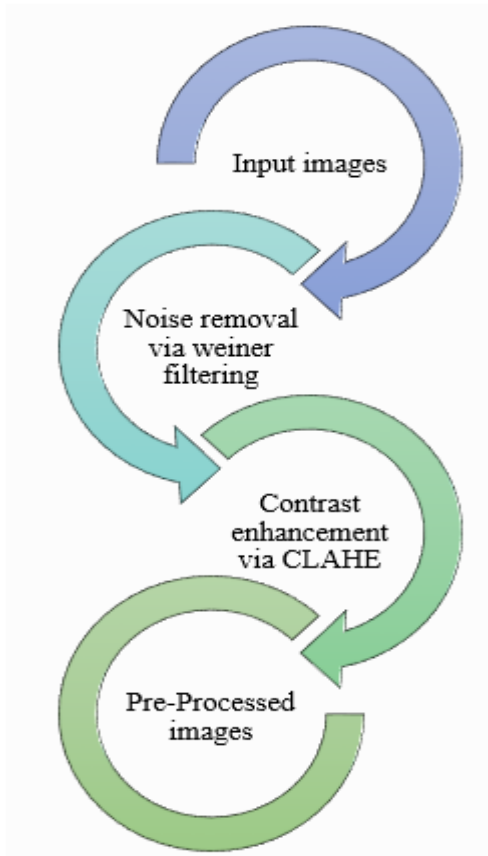


Fig. 3. Stages of pre-processing

ROI Identification

The ROI region in img^{pre} is isolated from the non-ROI using the Optimized K-Means clustering model. In img^{pre} , there is ROI img^{ROI} and Non-Region of Interest img^{ROI-N} . This img^{ROI-N} enhances the computational time, and therefore it is ought to be removed. The notion of segmenting image pixels into a set of organizations or regions depending on resemblance features is amongst the most popular ROI detection techniques. The cluster analysis algorithm K-means is an unsupervised learning algorithm. It's a method of classifying items into homogeneous groups called clusters depending on commonalities among them. It addresses the well-known clustering issue by taking into account specific qualities and using an iterative alternating matching procedure. The sensitivity of k-means clustering to initial centroids centre placements is its fundamental problem. By employing applying the projected Optimized K-Means clustering model this shortcomings of the traditional version is solved. The global minimum of the k-means cluster is found using this technique, which identifies the

optimal centres for each cluster. The following are the steps considered in the Optimized K-Means clustering model:

Step1: The set of clusters is determined by the variable K.

Step2: Pick K points or centroids optimally using the newly projected Dingo with Enhanced Encircling Optimization Model (DEEO) model, instead of random selection. This optimal selection of centroids enhances the performance of the model, by precisely identifying the ROI zones.

Step3: Allocate every data point towards the optimal centroid that is adjacent to it, forming the predetermined K clusters.

Step4: Compute the variance and reposition each cluster's centroid.

Step5: Resume the third steps, reassigning every data point to the cluster's new nearest centroid.

Step6: If there is a relocation, move to step 4; else Terminate

Step7: Terminate

The isolated ROI region is denoted as img^{ROI} .

Feature Extraction

The features like colour feature $g(color)$, texture features $g(texture)$ LBP [51]- Median Local Gradient Pattern (MLGP)) are extracted from img^{ROI} . This phase is diagrammatically shown in Fig.4.

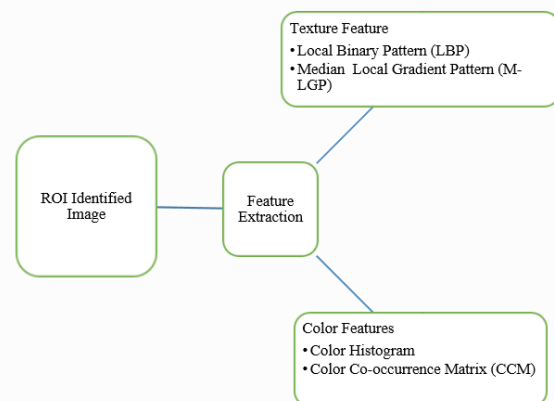


Fig. 4. Feature Extraction

colour feature : the colour features like Colour Histogram and Colour Co-occurrence Matrix (CCM) are extracted from img^{ROI} . The extracted colour features are together represented as $g(color)$.

Colour Histogram: One of most extensively used approach for obtaining the colour component of an image is indeed the colour histogram. It portrays the picture from a unique viewpoint, and shows how colour bins in such an image are distributed in terms of intensity. The colour histogram is simple to calculate and therefore is unaffected by tiny image alterations. The computed Colour Histogram features is denoted as g^{CH} .

CCM: the Colour co-occurrence matrix approach computes the colour variation among consecutive pixels of the image. Pixels make up a image, and every pixels represents 4 adjacent pixels colours. The computed features is denoted as g^{CCM} . The retrieved colour features is pointed as $g(color)$, and it is the combination of g^{CCM} hand g^{CH} .

Texture Features: the texture features like LBP and MLGP are extracted from img^{ROI}

LBP: it is a simple texture operator that is efficient in identifying the image pixels by means of thresholding each pixel's neighbourhood and converting the outcome to a binary integer. Mathematically, LBP can be given as per Eq. (2) and Eq. (3), respectively.

$$g^{LBP} = \sum_{i=0}^{Q-1} S(N_i - G).2^i$$

(2)

$$S(z) = \begin{cases} 1 & \text{if } z > 0 \\ 0 & \text{else} \end{cases}$$

(3)

Here, Q is the count of pixels of img^{ROI} and N_i is the count of neighbours and G is the value of eight neighbouring pixels.

MLGP : LGP is indeed a “dynamic threshold-based feature descriptor” for image classification that captures variations in levels of intensity locally or globally. The “Arithmetic Mean (AM)” of the gradient measures of neighbouring pixels is used to compute this boundary. Because of the use of AM, this value is frequently unable to decrease the influence of anomalies. As a result, some image components have been incorrectly detected. thus, LGP's discriminating capability is weaker than that of other descriptions in such a wide range of applications. Hence, in order to sort out this problem, we propose a new “median-based feature descriptor” called MLGP to replace LGP. An illustration of this model is shown in Fig.5. The steps followed in

MLGP is manifested below: 1. Within 3X3 matrix, the neighbouring pixels of img^{ROI} pixel are considered.

2. The values of the mid square is used as the centre pixel

3. The intensity differential between the centre and neighbouring pixels is calculated.

4. The median value (instead of AM in standard LGP) for all pixels in img^{ROI} with in 3X3 matrix is again calculated.

5. The median value replaces the original centre pixel value.

6. It had been contrasted to the pixels inside the matrix.

7. If indeed the values of the associated pixel seems to be greater than the values of the centre pixel, 1 would be inserted in the new matrix; otherwise, 0. Mathematically, MLGP can be given as per Eq. (4) and Eq. (5), respectively

$$g_{N,R}^{MLGP} = \sum_{i=0}^{N-1} S(C_i - C_{median}).2^i$$

(4)

$$S(h) = \begin{cases} 1 & \text{if } h > 0 \\ 0 & \text{else} \end{cases}$$

(5)

Here, R is the radius and h is the difference between the threshold, C_i is the gradient of the pixel and C_{median} is the median of neighbouring pixels N .

8. A binary pattern has been created in this manner.

9. The comparable decimal number is determined from binary pattern, and the centre pixels is updated. The retrieved texture features is pointed as $g(texture)$

These extracted features are together denoted as $G = g(texture) + g(color)$

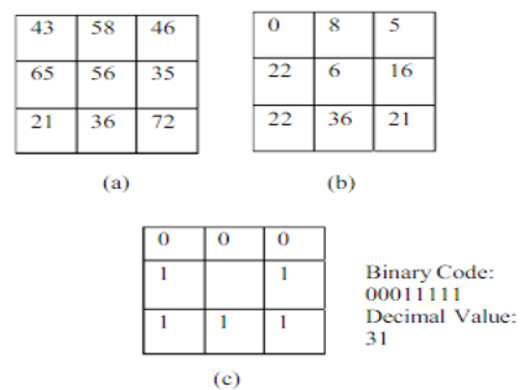


Fig. 5. MLGP model- (a) sample original image data, (b) computed median value and (c) MLGP value

Feature Selection-Dingo with Enhanced Encircling Optimization Model (DEEO)

The DEEO model is an extended version of standard DOX[52] model. This DEEO model includes three major phases: “(a) Enhanced Encircling phase, (b) Hunting phase and (c) Attacking prey phase”. The steps followed in DEEO model is manifested below:

Step1: The population of M search agents (dingo’s) are initialized. The population of the search agent is pointed as $G_i = i = 1, 2, \dots, m$. Here, the position of the search agent denotes the extracted features. The current iteration is denoted as itr and the maximal iteration is denoted as \max^{itr} . The input to DEEO model is G (extracted features) and the outcome from it is the optimal feature G^{opt} . Set G_α as the search agent with best search capability and G_β as the second best search and G_γ as the third best search agent.

Step2: Check the termination criterion: while $itr < \max^{itr}$ move to step 3, else terminate

Step3: The fitness function (fit) of every search agent is computed as per Eq. (6). The fitness function of this research work is the minimization of the classification errors E^{error}

$$Fit = \min(E^{error}) \quad (6)$$

Step4: Enhanced Encircling Phase- the search agent needs to efficient in finding the optimal solutions. Once, the location of the best solution (optimal feature) is identified, its position is encircled. For the enhancement of convergence of solutions, a new weight function W (proposed) is added. This W is computed using the chaotic map. This behaviour of the search agent is mathematically given in Eq.(7) to Eq. (11), respectively.

$$G = |A.Pos_p(z) - Pos(itr)| * W \quad (7)$$

$$Pos(itr + 1) = Pos_p(i) - b.G \quad (8)$$

$$A = 2.a \quad (9)$$

$$b = 2.B.a - B \quad (10)$$

$$B = 3 - \left[itr * \left(\frac{3}{\max^{itr}} \right) \right] \quad (11)$$

The value of $A = [1, 0], b = [1, 1]$. In addition, a, b is a control parameter (proposed) that can be computed as per Eq. (12) and Eq. (13), respectively.

$$a = 2^{(1-itr / \max^{itr})} \quad (12)$$

$$b = 2 - \left(\frac{2.itr}{\max^{itr}} \right) \quad (13)$$

Step5: Proposed Hunting Phase- Once the target prey (optimal feature) is encircled by the search agent, it encircles the prey and attacks it. G_α commands the hunting process and G_β, G_γ participate in hunting. Mathematically, this can be given as per Eq. (14)- Eq. (20), respectively. Here, $\omega(itr)$ is the newly added penalty function that changes with the count of iterations. This $\omega(itr)$ is added in order to prevent the solution from getting trapped into the local optima. The notation pos_α, pos_β and pos_γ points to the position of α, β, γ search agents, respectively. In addition, $pos(1), pos(2)$ and $pos(3)$ denotes the best position of α, β, γ search agents, respectively.

$$G_\alpha = |A.pos_\alpha - pos(1)| * \omega(itr) \quad (14)$$

$$G_\beta = |A.pos_\beta - pos(2)| * \omega(itr) \quad (15)$$

$$G_\gamma = |A.pos_\gamma - pos(3)| * \omega(itr) \quad (16)$$

$$pos(1) = |pos_\alpha - b.G_\alpha| \quad (17)$$

$$pos(2) = |pos_\beta - b.G_\beta| \quad (18)$$

$$pos(3) = |pos_\gamma - b.G_\gamma| \quad (19)$$

$$\omega(itr) = itr \sqrt{itr} \quad (20)$$

Step 6: Attacking Prey-In the attacking prey phase, B is decreased linearly. As a consequence, the optimal feature is identified.

Step 7: Enhance the current iteration rate by 1.

Step 8: End while (termination criterion)

Step 9: Return G^{opt}

Glaucoma Detection with Improved CNN

The classification of OC and OD for healthy and diseased takes place at this stage. The classification is accomplished via Improved CNN model (I-CNN). This Improved CNN is trained with G^{opt} . As a resultant, the outcome from Improved CNN exhibits the state of OC and OD (i.e. diseased or healthy).

Improved CNN: The Improved CNN is modelled with two segments: “encoder and decoder”. The encoder extracts the feature maps of G^{opt} and decoder provides the classified outcome. The encoder uses the training set’s image inputs, whereas the decoder uses

encoder pooling layers' sparse max-pooling indices. This design significantly decreases the amount of training data and up-samples to map pixel-wise categorisation using the encoder's pooling indices. The "VGG-16 network's first 13 convolution layers" are followed by the "batch normalised layer, an activation function, the pooling layer, and dropout units" in the aforementioned encoder. "Up-sampling layers, de-convolution layers, activation functions, batch normalised layers, dropout layers, and a multi-class soft-max classifier layer make up the decoder network". As a consequence, the CNN decoder has "13 de-convolution layers". The decoder's computations are fed into a multi-class soft-max classifiers, which outputs the probability for each class for each pixel separately. The network begins with just an input image training process and gradually moves throughout the network towards the ultimate layers. Mathematically, the convolutional Layer is computed as per Eq. (21).

$$X_j^l = f\left(\sum_{i \in M_j}^{l-1} X_i^{l-1} * K_{ij}^l + bias_j^i\right)$$

(21)

Here, X_j^l is the outcome from j^{th} convolutional layer of l^{th} channel. $f(.)$ is the activation function and M_j is the input feature map and $bias_j^i$ is the bias function and K_{ij}^l is the convolutional kernel. Between two convolutional layers, a "pooling layer" is usually sandwiched. The greatest value of the image area is pooled as the area's max pooling value, which keeps the texture of the image effectively. Cross-entropy loss is a popular loss function in classification problems. It displays how far two probability distributions are apart. Instead of computing the cross-entropy based loss function, the Mean Bias Error (MBE) loss function is used for efficient image classification. MBE mainly used to calculate the average bias in the CNN model. MBE mainly used to calculate the average bias in the CNN model.

Result and Discussion

Experimental Setup

The projected glaucoma detection model from retinal images has been implemented in MATLAB. The projected model has been validated with the dataset collected from : **Drishiti-GS - RETINA DATASET FOR ONH SEGMENTATION**

(<https://www.kaggle.com/datasets/lokeshsaipur/eddi/drishitigs-retina-dataset-for-onh-segmentation/code>) and RIM-ONE Release 3 dataset (["http://medimrg.webs.ull.es/research/retinal-imaging/rim-one/"](http://medimrg.webs.ull.es/research/retinal-imaging/rim-one/)) . The sample image and their corresponding pre-processing and segmentation phases are manifested in Fig. 6. among the collected data, 70% of the information has been used for training purpose and the rest 30% has been used for testing purpose. The projected model (Improved CNN with DEEO) has been compared over the existing models like CNN, RNN, CNN with DOX, Improved CNN with DOX, RNN with DOX and NN with DOX, respectively. The evaluation has been made in terms of "accuracy, specificity, sensitivity, precision and MCC", respectively. All the evaluations has been made by varying the Training Percentage (TP).

	Drishiti-GS Dataset	RIM-ONE Release 3 dataset
--	----------------------------	----------------------------------

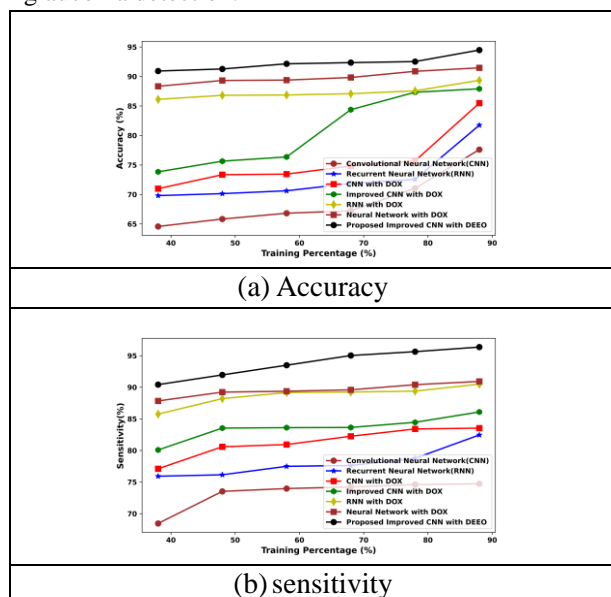
	Healthy	Diseased	Healthy	Diseased
Ground Truth				
Input image				
Pre-processed image-CLAHE				
Optimized K-means based segmentation for ROI identification				
Outcome				

Fig. 6. Sample Images of “Drishti-GS Dataset and RIM-ONE Release 3 dataset”

Performance analysis on Drishti-GS dataset

The outcomes acquired by the projected model for Drishti-GS dataset is shown in Fig. 7. On analysing the acquired outcomes, the projected model has recorded the highest accuracy rate for every variation in the TP. Moreover, the highest accuracy of 99.8% at 90th TP by the projected model. The precision identification of the ROI regions with DEEO based K-means Segmentation models has assisted in boosting the detection accuracy of the projected model. The sensitivity has been the most challenge faced by the existing works [1] [2] [5] [17]. This challenge has been overcome in this research work. The projected model has recorded the highest sensitivity than the existing models under every variation in TP. At 90th T, the projected model has recorded the highest sensitivity as 99.9%, which is indeed the most favourable score. The specificity of the projected model is also higher with the projected model over the existing models. The highest specificity of the projected model is TP=40 is 95%, TP=50 is 94%, TP=60 is 96%, TP=70 is 97.5%, TP=80 is 98% and TP=90 is 99.85%. Moreover, at 90th TP, the highest precision of 99.8% has been recorded by the projected model, which is better than existing models like CNN=90%, RNN=86%, CNN with DOX=85%, Improved CNN with DOX=84%, RNN with DOX=83% and NN with DOX=75%,

respectively. In addition, the projected model has also recorded the highest MCC as 99.7% at 90th TP, which is better than existing models like CNN=90%, RNN=89%, CNN with DOX=85%, Improved CNN with DOX=78%, RNN with DOX=76% and NN with DOX=98%, respectively. The major reason behind this enhancement is due to the selection of the optimal features with DEEO model. As a whole, the projected model is said to be much applicable for glaucoma detection.



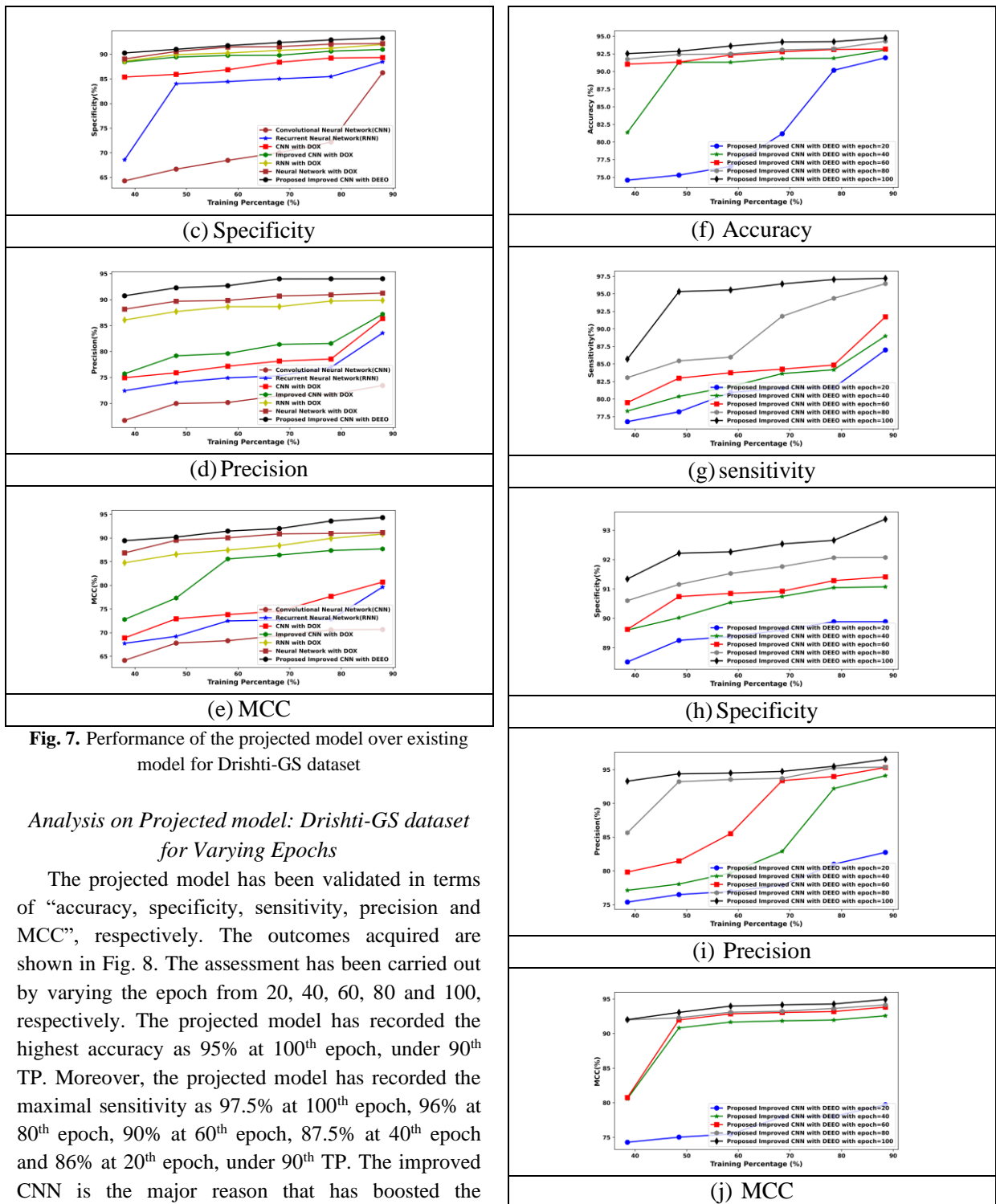


Fig. 7. Performance of the projected model over existing model for Drishti-GS dataset

Analysis on Projected model: Drishti-GS dataset for Varying Epochs

The projected model has been validated in terms of “accuracy, specificity, sensitivity, precision and MCC”, respectively. The outcomes acquired are shown in Fig. 8. The assessment has been carried out by varying the epoch from 20, 40, 60, 80 and 100, respectively. The projected model has recorded the highest accuracy as 95% at 100th epoch, under 90th TP. Moreover, the projected model has recorded the maximal sensitivity as 97.5% at 100th epoch, 96% at 80th epoch, 90% at 60th epoch, 87.5% at 40th epoch and 86% at 20th epoch, under 90th TP. The improved CNN is the major reason that has boosted the performance the projected model. Moreover, the specificity of the projected model under 90th TP is 87% at 20th epoch, 89% at 40th epoch, 91% at 60th TP, 92% at 80th epoch and 95% at 100th epoch. As a whole, the projected model is said to be the most optimal model for glaucoma detection.

Fig. 8. Performance of the projected model for Drishti-GS dataset: Under varying epoches

Fig. 9.

Performance Analysis on RIM-ONE Release 3 dataset

The evaluation of the projected model is made in terms of “accuracy, specificity, sensitivity, precision and MCC”, respectively. The outcomes acquired are shown in Fig. 9. On analysing the recorded outcome,

the projected model has recorded the best performance over the existing models for every variation in the TP. The extraction of the texture features as well as colour features for training the detection model has assisted in enhancing the detection performance of the suggested model. The projected model has recorded the highest accuracy for every variation in TP. The highest accuracy recorded by the projected model is 90% at 20th TP, 91% at 40% TP, 92% at 50th TP, 92.5% at 60th TP, 93% at 80th TP and 94% at 90th TP. The ROI identification with DEEO+K-means model is the major reason behind this performance enhancement. In addition, the projected model has recorded the highest sensitivity for every variation in TP, and this is evident from the results shown graphically. The highest sensitivity of 95% has been recorded by the projected model at TP=90 as 95.6%. In addition, the specificity of the projected model has been increased to 98%, and this is due to the selection for the optimal features with DEEO model. In addition, the precision of the projected model at 20th TP is 94%, which is better than CNN=75%, RNN=75%, CNN with DOX=80%, Improved CNN with DOX=84%, RNN with DOX=87% and NN with DOX=89%, respectively. Thus, the projected model is said to be much significant for glaucoma detection.

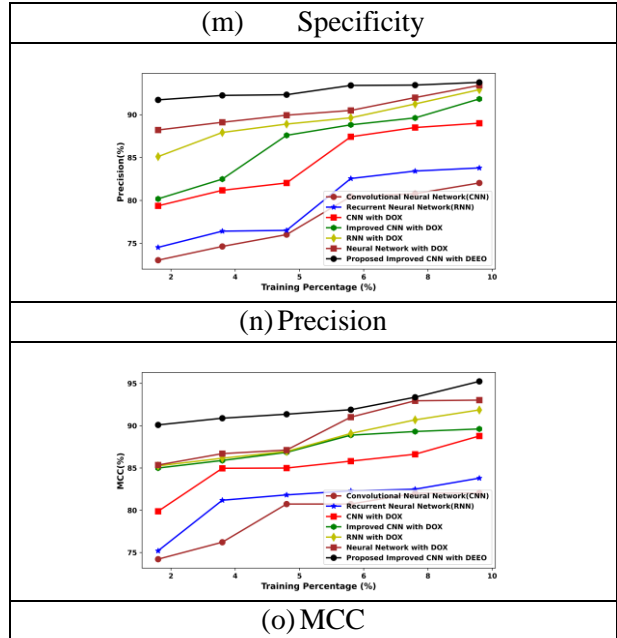
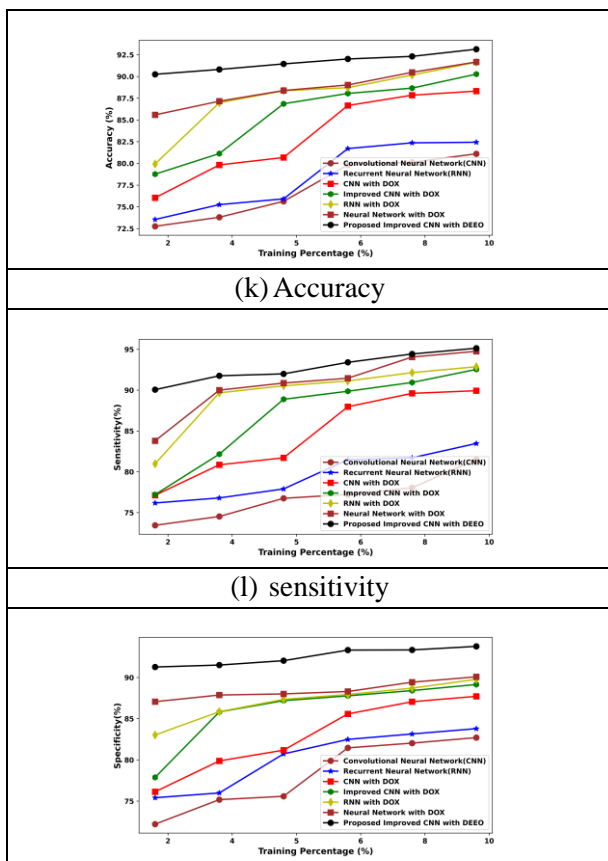
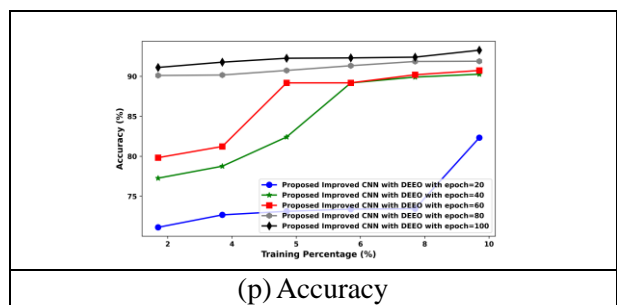


Fig. 10. Performance of the projected model over existing model for RIM-ONE Release 3 dataset

Analysis on Projected model: RIM-ONE Release 3 dataset for Varying Epochs

The outcomes acquired are shown in Fig. 10. The projected model has been validated for varying epochs. The projected model has recorded the highest accuracy as 98% at 100th epoch corresponding to 90th TP. In addition, the projected model has recorded the highest specificity, precision, sensitivity as well as MCC at 100th epoch. The sensitivity value recorded by the projected model at 20th TP is 70% at 20th epoch, 72% at 40th epoch, 80% at 60th epoch, 83% at 80th epoch and 95% at 100th epoch. In addition, the highest specificity of 98% is recorded by the projected model at 100th epoch corresponding to 90th TP. The precision value recorded by the projected model at 20th TP is 70%, 76%, 80%, 90% and 94% at 20th, 40th, 60th, 80th and 100th epoch, respectively. The improved CNN has assisted in enhancing the performance of the suggested model. As a whole, the projected model has been said to be efficient for glaucoma detection.



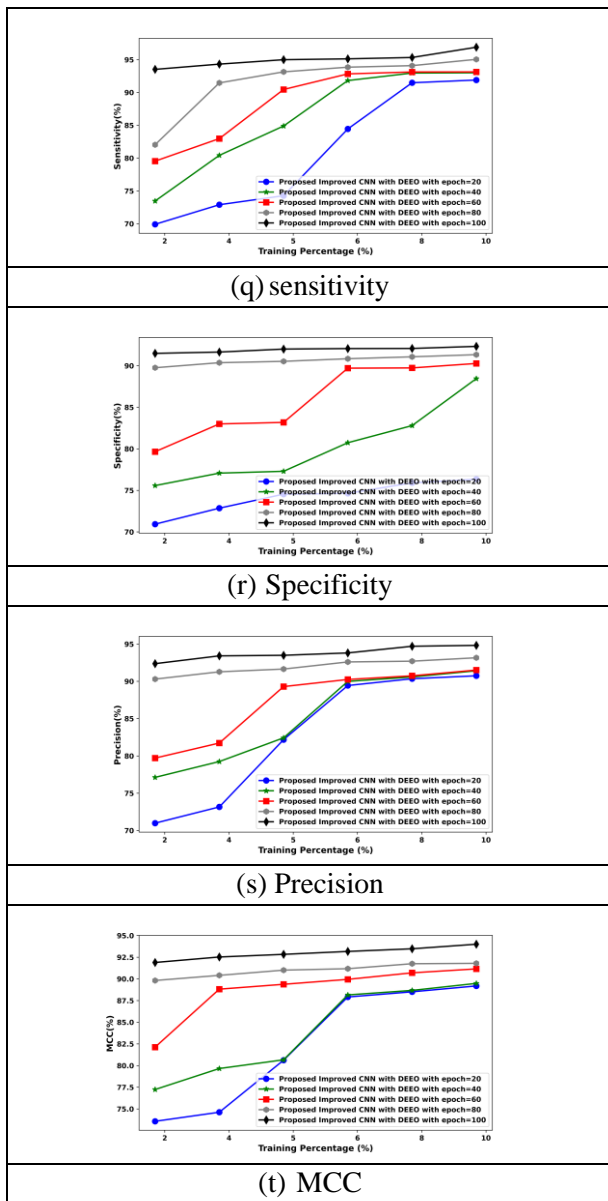


Fig. 11. Performance of the projected model for RIM-ONE Release 3 dataset : Under varying epochs

Conclusion

This paper has developed a novel glaucoma detection model. Initially, the collected retinal images were pre-processed via wiener filtering and CLAHE. Then, Region of Interest (ROI) of pre-processed image were selected via Optimized K-Means clustering technique, wherein the centroids of K-means are optimally selected DEEO. Subsequently, the features inclusive of color feature (Color Histogram and CCM), texture features (LBP, MLGP) were extracted from the identified ROI areas. Further, among the selected features, the most relevant features were selected via DEEO. Ultimately, using the I-CNN, the classification of OC and OD for healthy and diseased takes place precisely. Finally, a

comparative evaluation is undergone to validate the efficiency of the projected model. On analyzing the acquired outcomes, the projected model has recorded the highest accuracy rate for every variation in the TP. Moreover, the highest accuracy of 99.8% at 90th TP by the projected model for Drishti-GS dataset. The precision identification of the ROI regions with DEEO based K-means Segmentation models has assisted in boosting the detection accuracy of the projected model.

References

- [1] H. N. Veena, A. Muruganandham, T. Senthil Kumaran, "A novel optic disc and optic cup segmentation technique to diagnose glaucoma using deep learning convolutional neural network over retinal fundus images", *Journal of King Saud University - Computer and Information Sciences*, 2021
- [2] Akshat Tulsani, Preetham Kumar, Sumaiya Pathan, "Automated segmentation of optic disc and optic cup for glaucoma assessment using improved UNET++ architecture", *Biocybernetics and Biomedical Engineering*, 2021
- [3] Bingyan Liu, Daru Pan, Hui Song, "ECSD-Net: A joint optic disc and cup segmentation and glaucoma classification network based on unsupervised domain adaptation", *Computer Methods and Programs in Biomedicine*, 2021
- [4] Amed Mvoulana, Rostom Kachouri, Mohamed Akil, "Fully automated method for glaucoma screening using robust optic nerve head detection and unsupervised segmentation based cup-to-disc ratio computation in retinal fundus images", *Computerized Medical Imaging and Graphics*, 2020
- [5] José Escorcia-Gutierrez, Jordina Torrents-Barrena, Domènec Puig, "A color fusion model based on Markowitz portfolio optimization for optic disc segmentation in retinal images", *Expert Systems with Applications*, 2021
- [6] D. Parashar and D. K. Agrawal, "Automated Classification of Glaucoma Stages Using Flexible Analytic Wavelet Transform From Retinal Fundus Images," in *IEEE Sensors Journal*, vol. 20, no. 21, pp. 12885-12894, 1 Nov.1, 2020. doi: 10.1109/JSEN.2020.3001972
- [7] D. Parashar and D. K. Agrawal, "Automated Classification of Glaucoma Stages Using Flexible Analytic Wavelet Transform From Retinal Fundus Images," in *IEEE Sensors Journal*, vol. 20, no. 21, pp. 12885-12894, 1 Nov.1, 2020. doi: 10.1109/JSEN.2020.3001972

- [8] Y. George, B. J. Antony, H. Ishikawa, G. Wollstein, J. S. Schuman and R. Garnavi, "Attention-Guided 3D-CNN Framework for Glaucoma Detection and Structural-Functional Association Using Volumetric Images," in *IEEE Journal of Biomedical and Health Informatics*, vol. 24, no. 12, pp. 3421-3430, Dec. 2020. doi: 10.1109/JBHI.2020.3001019
- [9] D. Song *et al.*, "Deep Relation Transformer for Diagnosing Glaucoma With Optical Coherence Tomography and Visual Field Function," in *IEEE Transactions on Medical Imaging*, vol. 40, no. 9, pp. 2392-2402, Sept. 2021. doi: 10.1109/TMI.2021.3077484
- [10] M. Alghamdi and M. Abdel-Mottaleb, "A Comparative Study of Deep Learning Models for Diagnosing Glaucoma From Fundus Images," in *IEEE Access*, vol. 9, pp. 23894-23906, 2021. doi: 10.1109/ACCESS.2021.3056641
- [11] M. T. Islam, S. T. Mashfu, A. Faisal, S. C. Siam, I. T. Naheen and R. Khan, "Deep Learning-Based Glaucoma Detection With Cropped Optic Cup and Disc and Blood Vessel Segmentation," in *IEEE Access*, vol. 10, pp. 2828-2841, 2022. doi: 10.1109/ACCESS.2021.3139160
- [12] S. M. Shankaranarayana, K. Ram, K. Mitra and M. Sivaprakasam, "Fully Convolutional Networks for Monocular Retinal Depth Estimation and Optic Disc-Cup Segmentation," in *IEEE Journal of Biomedical and Health Informatics*, vol. 23, no. 4, pp. 1417-1426, July 2019. doi: 10.1109/JBHI.2019.2899403
- [13] M. Tabassum *et al.*, "CDED-Net: Joint Segmentation of Optic Disc and Optic Cup for Glaucoma Screening," in *IEEE Access*, vol. 8, pp. 102733-102747, 2020. doi: 10.1109/ACCESS.2020.2998635
- [14] K. A. Thakoor, S. C. Koorathota, D. C. Hood and P. Sajda, "Robust and Interpretable Convolutional Neural Networks to Detect Glaucoma in Optical Coherence Tomography Images," in *IEEE Transactions on Biomedical Engineering*, vol. 68, no. 8, pp. 2456-2466, Aug. 2021. doi: 10.1109/TBME.2020.3043215
- [15] P. Syga, C. Sielużycki, P. Krzyżanowska-Berkowska and D. R. Iskander, "A Fully Automated 3D In-Vivo Delineation and Shape Parameterization of the Human Lamina Cribrosa in Optical Coherence Tomography," in *IEEE Transactions on Biomedical Engineering*, vol. 66, no. 5, pp. 1422-1428, May 2019. doi: 10.1109/TBME.2018.2873893
- [16] S. Wang, L. Yu, X. Yang, C. -W. Fu and P. -A. Heng, "Patch-Based Output Space Adversarial Learning for Joint Optic Disc and Cup Segmentation," in *IEEE Transactions on Medical Imaging*, vol. 38, no. 11, pp. 2485-2495, Nov. 2019. doi: 10.1109/TMI.2019.2899910
- [17] J. Guo, G. Azzopardi, C. Shi, N. M. Jansonius and N. Petkov, "Automatic Determination of Vertical Cup-to-Disc Ratio in Retinal Fundus Images for Glaucoma Screening," in *IEEE Access*, vol. 7, pp. 8527-8541, 2019. doi: 10.1109/ACCESS.2018.2890544
- [18] R. Ali *et al.*, "Optic Disk and Cup Segmentation Through Fuzzy Broad Learning System for Glaucoma Screening," in *IEEE Transactions on Industrial Informatics*, vol. 17, no. 4, pp. 2476-2487, April 2021. doi: 10.1109/TII.2020.3000204
- [19] T. Khalil, M. U. Akram, H. Raja, A. Jameel and I. Basit, "Detection of Glaucoma Using Cup to Disc Ratio From Spectral Domain Optical Coherence Tomography Images," in *IEEE Access*, vol. 6, pp. 4560-4576, 2018. doi: 10.1109/ACCESS.2018.2791427
- [20] S. Lu, M. Hu, R. Li and Y. Xu, "A Novel Adaptive Weighted Loss Design in Adversarial Learning for Retinal Nerve Fiber Layer Defect Segmentation," in *IEEE Access*, vol. 8, pp. 132348-132359, 2020. doi: 10.1109/ACCESS.2020.3009442
- [21] Y. Gao, X. Yu, C. Wu, W. Zhou, X. Wang and H. Chu, "Accurate and Efficient Segmentation of Optic Disc and Optic Cup in Retinal Images Integrating Multi-View Information," in *IEEE Access*, vol. 7, pp. 148183-148197, 2019. doi: 10.1109/ACCESS.2019.2946374
- [22] X. Qian *et al.*, "In Vivo Visualization of Eye Vasculature Using Super-Resolution Ultrasound Microvessel Imaging," in *IEEE Transactions on Biomedical Engineering*, vol. 67, no. 10, pp. 2870-2880, Oct. 2020. doi: 10.1109/TBME.2020.2972514
- [23] J. Cheng, Z. Li, Z. Gu, H. Fu, D. W. K. Wong and J. Liu, "Structure-Preserving Guided Retinal Image Filtering and Its Application for Optic Disk Analysis," in *IEEE Transactions on Medical Imaging*, vol. 37, no. 11, pp. 2536-2546, Nov. 2018. doi: 10.1109/TMI.2018.2838550
- [24] Y. Jiang *et al.*, "JointRCNN: A Region-Based Convolutional Neural Network for Optic Disc and Cup Segmentation," in *IEEE Transactions on Biomedical Engineering*, vol. 67, no. 2, pp. 335-343,

- Feb. 2020.
doi: 10.1109/TBME.2019.2913211
- [25] H. Fu, J. Cheng, Y. Xu, D. W. K. Wong, J. Liu and X. Cao, "Joint Optic Disc and Cup Segmentation Based on Multi-Label Deep Network and Polar Transformation," in *IEEE Transactions on Medical Imaging*, vol. 37, no. 7, pp. 1597-1605, July 2018.
doi: 10.1109/TMI.2018.2791488
- [26] R. Zhao, X. Chen, X. Liu, Z. Chen, F. Guo and S. Li, "Direct Cup-to-Disc Ratio Estimation for Glaucoma Screening via Semi-Supervised Learning," in *IEEE Journal of Biomedical and Health Informatics*, vol. 24, no. 4, pp. 1104-1113, April 2020.
doi: 10.1109/JBHI.2019.2934477
- [27] S. M. Shankaranarayana, K. Ram, K. Mitra and M. Sivaprakasam, "Fully Convolutional Networks for Monocular Retinal Depth Estimation and Optic Disc-Cup Segmentation," in *IEEE Journal of Biomedical and Health Informatics*, vol. 23, no. 4, pp. 1417-1426, July 2019.
doi: 10.1109/JBHI.2019.2899403
- [28] M. Tabassum *et al.*, "CDED-Net: Joint Segmentation of Optic Disc and Optic Cup for Glaucoma Screening," in *IEEE Access*, vol. 8, pp. 102733-102747, 2020.
doi: 10.1109/ACCESS.2020.2998635
- [29] S. Wang, L. Yu, X. Yang, C. -W. Fu and P. -A. Heng, "Patch-Based Output Space Adversarial Learning for Joint Optic Disc and Cup Segmentation," in *IEEE Transactions on Medical Imaging*, vol. 38, no. 11, pp. 2485-2495, Nov. 2019.
doi: 10.1109/TMI.2019.2899910
- [30] R. Ali *et al.*, "Optic Disk and Cup Segmentation Through Fuzzy Broad Learning System for Glaucoma Screening," in *IEEE Transactions on Industrial Informatics*, vol. 17, no. 4, pp. 2476-2487, April 2021.
doi: 10.1109/TII.2020.3000204
- [31] F. Abdullah *et al.*, "A Review on Glaucoma Disease Detection Using Computerized Techniques," in *IEEE Access*, vol. 9, pp. 37311-37333, 2021.
doi: 10.1109/ACCESS.2021.3061451
- [32] T. Khalil, M. U. Akram, H. Raja, A. Jameel and I. Basit, "Detection of Glaucoma Using Cup to Disc Ratio From Spectral Domain Optical Coherence Tomography Images," in *IEEE Access*, vol. 6, pp. 4560-4576, 2018.
doi: 10.1109/ACCESS.2018.2791427
- [33] M. T. Islam, S. T. Mashfu, A. Faisal, S. C. Siam, I. T. Naheen and R. Khan, "Deep Learning-Based Glaucoma Detection With Cropped Optic Cup and Disc and Blood Vessel Segmentation," in *IEEE Access*, vol. 10, pp. 2828-2841, 2022.
doi: 10.1109/ACCESS.2021.3139160
- [34] Y. Gao, X. Yu, C. Wu, W. Zhou, X. Wang and H. Chu, "Accurate and Efficient Segmentation of Optic Disc and Optic Cup in Retinal Images Integrating Multi-View Information," in *IEEE Access*, vol. 7, pp. 148183-148197, 2019.
doi: 10.1109/ACCESS.2019.2946374
- [35] Y. Jiang, N. Tan and T. Peng, "Optic Disc and Cup Segmentation Based on Deep Convolutional Generative Adversarial Networks," in *IEEE Access*, vol. 7, pp. 64483-64493, 2019.
doi: 10.1109/ACCESS.2019.2917508
- [36] J. Civit-Masot, M. J. Domínguez-Morales, S. Vicente-Díaz and A. Civit, "Dual Machine-Learning System to Aid Glaucoma Diagnosis Using Disc and Cup Feature Extraction," in *IEEE Access*, vol. 8, pp. 127519-127529, 2020.
doi: 10.1109/ACCESS.2020.3008539
- [37] H. Lei, W. Liu, H. Xie, B. Zhao, G. Yue and B. Lei, "Unsupervised Domain Adaptation Based Image Synthesis and Feature Alignment for Joint Optic Disc and Cup Segmentation," in *IEEE Journal of Biomedical and Health Informatics*, vol. 26, no. 1, pp. 90-102, Jan. 2022.
doi: 10.1109/JBHI.2021.3085770
- [38] H. Raja, T. Hassan, M. U. Akram and N. Werghi, "Clinically Verified Hybrid Deep Learning System for Retinal Ganglion Cells Aware Grading of Glaucomatous Progression," in *IEEE Transactions on Biomedical Engineering*, vol. 68, no. 7, pp. 2140-2151, July 2021.
doi: 10.1109/TBME.2020.3030085
- [39] O. J. Afolabi, G. P. Mabuza-Hocquet, F. V. Nelwamondo and B. S. Paul, "The Use of U-Net Lite and Extreme Gradient Boost (XGB) for Glaucoma Detection," in *IEEE Access*, vol. 9, pp. 47411-47424, 2021.
doi: 10.1109/ACCESS.2021.3068204
- [40] M. Alghamdi and M. Abdel-Mottaleb, "A Comparative Study of Deep Learning Models for Diagnosing Glaucoma From Fundus Images," in *IEEE Access*, vol. 9, pp. 23894-23906, 2021.
doi: 10.1109/ACCESS.2021.3056641
- [41] F. Guo *et al.*, "Yanbao: A Mobile App Using the Measurement of Clinical Parameters for Glaucoma Screening," in *IEEE Access*, vol. 6, pp. 77414-77428, 2018.
doi: 10.1109/ACCESS.2018.2882946

- [42] J. Guo, G. Azzopardi, C. Shi, N. M. Jansonius and N. Petkov, "Automatic Determination of Vertical Cup-to-Disc Ratio in Retinal Fundus Images for Glaucoma Screening," in *IEEE Access*, vol. 7, pp. 8527-8541, 2019. doi: 10.1109/ACCESS.2018.2890544
- [43] J. Cheng, Z. Li, Z. Gu, H. Fu, D. W. K. Wong and J. Liu, "Structure-Preserving Guided Retinal Image Filtering and Its Application for Optic Disk Analysis," in *IEEE Transactions on Medical Imaging*, vol. 37, no. 11, pp. 2536-2546, Nov. 2018. doi: 10.1109/TMI.2018.2838550
- [44] S. -P. Xu, T. -B. Li, Z. -Q. Zhang and D. Song, "Minimizing-Entropy and Fourier Consistency Network for Domain Adaptation on Optic Disc and Cup Segmentation," in *IEEE Access*, vol. 9, pp. 153985-153994, 2021. doi: 10.1109/ACCESS.2021.3128174
- [45] J. Civit-Masot, F. Luna-Perejón, S. Vicente-Díaz, J. M. Rodríguez Corral and A. Civit, "TPU Cloud-Based Generalized U-Net for Eye Fundus Image Segmentation," in *IEEE Access*, vol. 7, pp. 142379-142387, 2019. doi: 10.1109/ACCESS.2019.2944692
- [46] J. Cheng, "Sparse Range-Constrained Learning and Its Application for Medical Image Grading," in *IEEE Transactions on Medical Imaging*, vol. 37, no. 12, pp. 2729-2738, Dec. 2018. doi: 10.1109/TMI.2018.2851607
- [47] M. N. Zahoor and M. M. Fraz, "A Correction to the Article "Fast Optic Disc Segmentation in Retina Using Polar Transform"," in *IEEE Access*, vol. 6, pp. 4845-4849, 2018. doi: 10.1109/ACCESS.2018.2790040
- [48] S. Khetkeeree and S. Liangrocapart, "Image Restoration Using Optimized Wiener Filtering Based on Modified Tikhonov Regularization," 2019 IEEE 4th International Conference on Signal and Image Processing (ICSIP), 2019, pp. 1015-1020, doi: 10.1109/SIPROCESS.2019.8868907.
- [49] B. K. Umri, M. Wafa Akhyari and K. Kusrini, "Detection of Covid-19 in Chest X-ray Image using CLAHE and Convolutional Neural Network," 2020 2nd International Conference on Cybernetics and Intelligent System (ICORIS), 2020, pp. 1-5, doi: 10.1109/ICORIS50180.2020.9320806.
- [50] A. Varghese, R. R. Varghese, K. Balakrishnan and J. S. Paul, "Level identification of brain MR images using histogram of a LBP variant," 2012 IEEE International Conference on Computational Intelligence and Computing Research, 2012, pp. 1-4, doi: 10.1109/ICCIC.2012.6510233
- [51] Amit Kumar Bairwa, Sandeep Joshi, and Dilbag Singh, "Dingo Optimizer: A Nature-Inspired Metaheuristic Approach for Engineering Problems", Hindawi, 2021